Seismic anisotropy in northern and central Gulf of California region, Mexico, from teleseismic receiver functions and new evidence of possible plate capture

Mathias Obrebski, Raúl R. Castro

Seismic anisotropy in northern and central Gulf of California region, Mexico, from teleseismic receiver functions and new evidence of possible plate capture

Mathias Obrebski[1,2] and Raúl R. Castro[1]

Received 4 May 2007; revised 31 October 2007; accepted 14 December 2007; published 1 March 2008.

[1] We present anisotropic models for the shallow lithosphere in the northern and central Gulf of California obtained from receiver function (RF) analysis. This region has undergone intense plate reorganization over the past 25 Ma that led to the transfer of the plate boundary east of the modern Baja California Peninsula posterior to the cease of the subduction of the Farallon plate beneath the North American plate. Our main interest in modeling the seismic anisotropy is to characterize rock fabric inherited from past and recent tectonism and to provide new information for understanding the tectonic processes involved in the evolution of the local plate boundary. We calculate RFs from teleseismic *P* waves recorded by the Network of Autonomously Recording Seismographs(NARS)-Baja array, and we stack them in 20° wide back azimuthal bins to enhance coherent information. These RFs yield significant transverse energy whose azimuthal variations are not consistent with that expected for a crust with dipping Moho. Therefore we interpret the conspicuous RFs energy of the transverse component as convincing evidence of anisotropy. We present forward models obtained by fitting the radial and transverse RFs with synthetic seismograms calculated with a reflectivity code. Our analysis suggests substantial variations in the structure of the shallow lithosphere along the Baja California Peninsula and the presence of stalled fragments of the extinct Farallon plate beneath its central part. The results at station NE81 in Sonora are interpreted as frozen crustal anisotropy inherited from Miocene Basin and Range extension, consistent with previous observations of the upper mantle anisotropy beneath this station.

Citation: Obrebski, M., and R. R. Castro (2008), Seismic anisotropy in northern and central Gulf of California region, Mexico, from teleseismic receiver functions and new evidence of possible plate capture, *J. Geophys. Res.*, *113*, B03301, doi:10.1029/2007JB005156.

1. Introduction

[2] The Gulf of California (GoC) and adjacent regions (Figure 1) encompass three structural provinces as described by *Stock et al.* [1991]. To the northwest, the Transpeninsular Strike-Slip Province is a diffuse element of the Pacific-North America plate boundary and transfers strain from the rift within the GoC to the faults on the continental borderland, west from the Baja California Peninsula. The Stable Central Peninsula displays a relatively unfaulted and unextended crust and no significant seismic activity. Finally, the Gulf Extensional Province is the site of most modern tectonism in its western side that hosts today's transtensional Pacific-North American plate boundary. The eastern side of the Gulf Extensional Province exhibits typical Basin-and-Range morphology, acquired mostly between ~27 and 12 Ma in southern Sonora [*Gans*, 1997] and 25–18 Ma in northern Sonora [*Nourse et al.*, 1994], though there are indications of modern tectonism with moderate rate [*Suter and Contreras*, 2002]. An extensive review of the geology of the whole GoC region was done by *Sedlock* [2003].

[3] The region under study constitutes a great natural laboratory to study mantle dynamics related to major tectonic processes such as the cessation of subduction, continental breakup and early stage of rifting. After the east margin of the Pacific Plate came into contact with the North American Plate about 25 Ma ago, the convergent margin, west from the modern Baja California Peninsula, progressively turned into a transform boundary as the Mendocino and Rivera triple junctions migrated northward and southward, respectively [*Atwater*, 1989]. The obliquity between the Pacific-North American relative plate motion and their common boundary is thought to have triggered extension in the former arc since middle Miocene and therefore forced the opening of the GoC. Nevertheless, the timing and location of strain since middle Miocene is still theme of

[1]Centro de Investigación Científica y de Educación Superior de Ensenada, Ensenada, Baja California, México.
[2]Now at Laboratoire de Sismologie, Institut de Physique du Globe de Paris, Paris, France.

0148-0227/08/2007JB005156$09.00

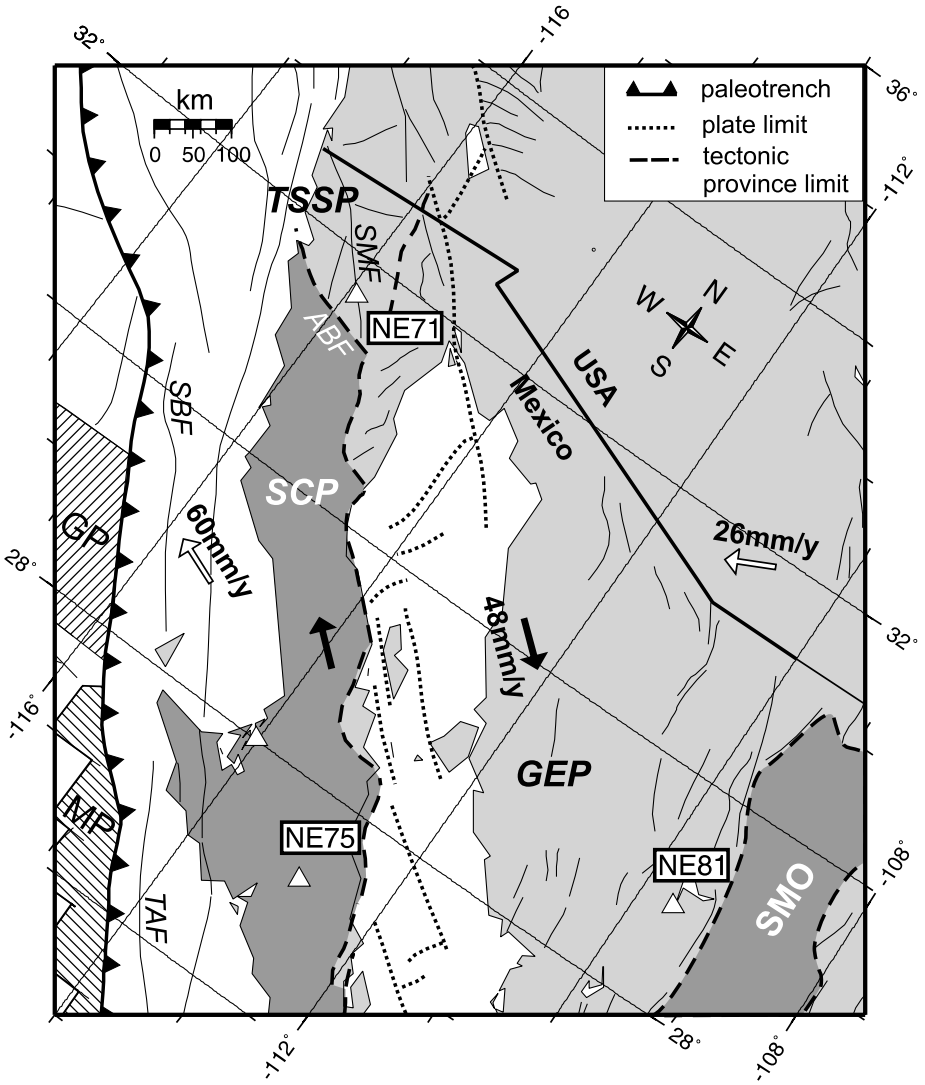

Figure 1. Tectonic map of the region under study. Gray areas represent land, and white areas represent water. Dark areas correspond to the Stable Central Peninsula (SCP) and the Sierra Madre Occidental (SMO) that are roughly unextended. The striped areas are the Guadalupe (GP) and Magdalena (MP) oceanic microplates. Also shown are the stations of NARS-Baja array at which we conducted our analysis. Thin lines represent faults. Paleotrench indicates the site where extinct Farallon was subducted beneath the continental margin. Dotted lines show the transform faults and dorsal segments that compose the Pacific-North American plate boundary, white arrows indicate the absolute plate motion of these two plates calculated from a hot spot reference, and the thick black arrows are their relative motion. Dashed lines represent the boundaries between the structural provinces as described by *Stock et al.* [1991]. ABF, Agua Blanca Fault; GEP, Gulf Extensional Province; SBF, San Benito Fault; SMF, San Miguel Fault; TAF, Tosco-Abreojos Fault; TSSP, Transpeninsular Strike-Slip Province.

debate. Several tectonic models [*Stock and Hodges*, 1989; *Oskin et al.*, 2001; *Bennett et al.*, 2007] state that the Pacific-North American divergent plate motion was first partitioned into NE-SW continental rifting in the former arc and NNW-SSW transform motion taken up along the San Benito-Tosco-Abreojos system (Figure 1). Then the tectonic activity may have vanished along this fault system and thus caused the whole Pacific-North American plate boundary to migrate into the GoC giving rise to oblique rifting and seafloor spreading since 5–6 Ma [*Lonsdale*, 1989; *Umhoefer et al.*, 1994]. In contrast, other models suggest that the opening of the GoC has occurred in one single phase [*Gans*, 1997; *Fletcher and Munguía*, 2000; *Sutherland et al.*, 2006, *Fletcher et al.*, 2007] and includes a limited amount of strain partitioning on either sides of the Baja California Peninsula [*Fletcher et al.*, 2007]. Other poorly understood issues that may have implications for the style, timing and locus of extension since middle Miocene within the GoC include its relation with the earlier intense period of extension and magmatic activity from Oligocene to middle Miocene on the east side of the Gulf Extensional Province [*Nourse et al.*, 1994; *Gans*,

Table 1. List of Events Used to Obtain Receiver Functions[a]

Origin						NE71		NE75		NE81	
Date (year/month/day)	Time (UT)	Latitude (deg)	Longitude (deg)	Depth (km)	M	Δ (deg)	baz (deg)	Δ (deg)	baz (deg)	Δ (deg)	baz (deg)
2002/04/26	1606:07	13.1	144.6	86	7.1	91.1	286.0	94.9	287.3	x	
2002/06/17	2126:23	−12.6	166.4	33	6.7	86.3	252.9	87.6	254.7	x	
2002/06/28	1719:30	43.8	130.7	566	7.3	83.4	318.0	88.4	319.5	x	
2002/08/02	2311:39	29.3	139.0	426	6.3	86.5	302.3	x		x	
2002/09/24	0357:22	−31.5	−69.2	119	6.3	76.8	140.3	71.7	141.6	x	
2002/10/04	1905:49	−21.0	−179.0	621	6.3	80.1	237.9	79.9	240.2	x	
2002/10/12	2009:11	−8.3	−71.7	534	6.9	57.9	125.6	53.2	125.7	x	
2002/10/17	0423:56	−19.8	−178.4	627	6.2	78.8	238.3	78.8	240.9	x	
2002/10/22	1139:04	−20.6	−178.4	549	6.2	79.2	237.7	x		x	
2002/10/23	1127:19	63.5	−147.9	4	6.7	37.6	337.1	42.7	337.7	42.3	335.7
2002/11/03	2212:41	63.5	−147.4	4	8.5	37.5	337.4	42.5	337.9	42.2	335.9
2002/11/17	0453:53	47.8	146.2	459	7.3	72.1	315.4	77.1	317.2	77.8	318.0
2002/11/20	2132:31	35.4	74.5	33	6.3	112.5	350.8	x		x	
2002/11/21	0253:15	12.4	−82.2	7	5.8	36.5	114.3	x		30.3	117.1
2002/12/23	1346:11	17.0	−85.6	33	6	31.1	111	x		25.0	113.1
2003/01/04	0515:04	−20.6	−177.7	378	6.5	78.7	237.3	x		81.9	241.3
2003/01/20	0843:06	−10.5	160.8	33	7.3	89.8	257.6	91.5	259.1	x	
2003/03/14	1254:12	−17.4	−175.2	274	6.4	74.9	238.2	x		x	
2003/04/27	2257:45	−8.2	−71.6	559	6.0	58.0	125.4	53.3	125.5	x	
2003/05/04	1315:19	−30.5	−178.2	62	6.7	85.5	230.0	84.8	232	x	
2003/05/14	0603:36	18.3	−58.6	41	6.7	53	90.2	50.4	88.2	x	
2003/05/19	1043:23	−18.0	−178.7	563	6.0	77.8	239.9	78.0	242.5	81.3	244
2003/05/26	0924:33	38.9	141.6	68	7.0	79.5	309.2	84.3	310.9	85.4	312.1
2003/05/26	1923:28	2.4	128.9	31	7.0	110.0	285.9	x		116.0	288.6
2003/05/26	2313:30	6.8	123.7	566	6.9	111.5	292.9	115.7	293.1	117.6	296.0
2003/06/16	2208:02	55.5	160.0	175	6.9	63.5	320.6	66.4	321.7	66.9	321.8
2003/06/20	0619:39	−7.6	−71.7	558	7.1	57.5	125.0	52.8	125.1	51.4	128.9
2003/07/27	0204:11	−21.1	−176.6	212	6.6	78.2	236.3	78.1	238.8	x	
2003/07/27	0625:32	47.2	139.2	470	6.8	76.5	317.3	81.5	319.0	x	
2003/07/27	1141:27	−20.1	−65.2	345	6.0	70.8	129.7	65.9	130.5	x	
2003/08/21	1212:50	−45.1	167.1	28	7.2	103.4	225.2	x		x	
2003/09/06	0208:14	−4.6	−106.0	10	6.1	37.5	163.7	x		33.4	174.1
2003/09/22	0445:36	19.8	−70.7	10	6.6	42.1	95.1	39.2	91.7	36.5	95.5
2003/09/27	1133:25	50.0	87.8	16	7.3	95.9	344.9	100.8	356.6	99.8	348.7
2003/10/01	0103:25	50.2	87.7	10	6.7	95.2	345.0	100.7	346.7	99.7	348.8
2003/10/15	0219:44	−17.8	−178.7	582	6.0	77.7	240.1	77.9	242.7	81.2	244.2
2003/11/12	0826:44	33.2	137.1	384	6.4	85.6	306.5	x		91.6	309.6
2003/12/01	0138:32	42.9	80.5	10	6.0	104.2	347.6	x		x	
2004/01/25	1143:12	−16.8	−174.2	129	6.7	73.8	238.0	73.8	241	77.1	242.5
2004/02/10	2033:51	59.4	−152.0	65	5.6	36.7	329.7	41.8	331.0	41.8	328.8
2004/03/12	2213:14	−15.6	−175.1	271	6.0	73.6	239.6	x		77.1	244.1
2004/03/17	0321:08	−21.1	−65.6	290	6.1	71.2	130.7	66.3	131.5	65.3	134.5
2004/04/05	2124:04	36.5	71.0	187	6.6	111.8	354.0	116.4	356.5	x	
2004/04/08	0457:50	−36.3	−97.8	10	6.4	x		64.7	166.6	65.7	169.6
2004/04/09	1523:35	−13.2	167.2	228	6.5	85.9	252.0	87.2	253.8	90.4	255.3
2004/04/11	1806:12	42.9	144.8	41	6.1	75.3	311.4	80.2	313.3	x	
2004/04/14	0133:05	−17.9	−174.6	143	6	74.7	237.5	x		78.0	241.9
2004/05/28	1238:44	36.2	51.6	17	6.3	111.4	10.8	115.1	13.8	112.8	16.4
2004/06/04	0148:03	54.5	−163.9	72	5.6	40.7	318.4	45.7	320.7	x	
2004/06/08	0855:53	17.5	−83.5	10	5.9	x		x		26.5	109.6
2004/06/10	1519:58	55.7	160.0	189	6.9	61.2	320.0	66.3	321.9	66.8	322.0
2004/07/01	0920:44	54.1	−35.3	10	5.6	x		x		58.1	41.9
2004/07/08	1954:34	−25.1	−116.0	10	6	x		x		54.0	187.1
2004/07/11	2346:12	−20.3	−126.9	12	6.1	52.7	193.0	49.1	197.6	51.6	200.8
2004/07/15	0427:15	−17.7	−178.8	565	7.1	77.0	241.1	77.9	242.9	x	
2004/08/01	1944:47	−13.4	−112.2	10	5.8	44.9	174.9	x		41.2	183.7
2004/08/10	0147:33	36.4	70.8	207	6.0	111.9	354.2	x		x	
2004/08/15	0341:17	−6.2	−107.2	10	5.6	x		x		35.0	175.7
2004/09/09	1633:22	17.8	−81.6	25	6	34	105.9	x		x	
2004/09/18	0707:48	23.1	−67.6	10	5.7	43.4	88.9	x		38.0	88.8
2004/10/08	0827:53	−11.0	162.2	36	6.8	88.9	256.5	90.5	258.0	93.6	259.5
2004/10/08	1436:06	13.9	120.6	105	6.5	109.4	308.0	x		x	
2004/10/15	0408:50	24.5	122.7	94	6.7	100.8	307.7	x		x	
2004/11/07	0202:26	48.0	144.5	474	6.2	73	316.1	x		78.7	318.8
2004/11/17	2109:13	−20.1	−178.7	622	6.6	79.1	238.4	79.2	240.8	x	
2004/11/21	1141:08	15.7	−61.7	14	6.3	51.6	94.8	48.6	82.8	x	
2004/11/28	0235:13	−26.5	−113.8	10	6.6	57.9	177.8	53.5	181.1	x	
2004/11/28	1832:14	43.0	145.1	39	7.0	75.0	311.4	79.9	313.2	x	
2004/12/06	1415:12	42.9	145.2	35	6.8	75.0	311.3	79.9	313.1	x	
2004/12/14	2320:13	19.0	−81.4	10	6.8	33.5	103.9	x		x	
2005/01/18	0659:04	57.1	−33.8	10	5.7	59.7	38.6	x		x	
2005/02/05	0334:26	16.0	145.9	143	7.0	88.5	287.8	92.4	289.3	x	

Table 1. (continued)

Origin						NE71		NE75		NE81	
Date (year/month/day)	Time (UT)	Latitude (deg)	Longitude (deg)	Depth (km)	M	Δ (deg)	baz (deg)	Δ (deg)	baz (deg)	Δ (deg)	baz (deg)
2005/02/05	1223:19	5.3	123.3	525	7.1	112.7	291.9	x		x	
2005/02/08	1448:22	−14.3	167.3	206	6.8	86.5	251.1	87.7	252.8	x	
2005/02/14	1805:59	15.8	−61.7	11	5.8	x		48.6	92.7	x	
2005/02/14	2338:09	41.7	79.4	22	6.1	105.6	348.1	x		x	
2005/03/19	1734:46	−21.9	−179.6	598	6.3	81.5	237.9	80.8	239.8	84.1	241.3
2005/03/21	1223:54	−25.0	−63.5	579	6.9	75.3	132.0	70.4	133.0	69.8	135.7
2005/03/30	1741:57	−22.5	−179.8	588	6.2	82.0	237.6	81.3	239.4	84.6	240.9
2005/04/11	1454:07	−7.3	−77.9	129	6.1	53.0	130.2	48.2	130.3	47.2	137.4
2005/06/02	1056:02	−24.2	−67.0	196	6.1	x		76.6	134.9	66.8	137.7
2005/06/13	2244:34	−20.0	−69.2	116	7.8	x		63.2	133.3	62.3	136.5

[a]Parameter Δ represents the epicentral distance, and "baz" represents the back azimuth at a singular station. A cross indicates that either the event misses the singular station database or the recorded seismic trace failed to provide a good receiver function, i.e., that yields a high signal-to-noise ratio and that proves consistent with other receiver functions with similar back azimuth.

1997] and the fate of the remnants of the Farallon slab after the cease of the subduction.

[4] The interest of studying seismic anisotropy stems in its tight relation with preferentially oriented features in rocks such as cracks or intrinsically anisotropic minerals [*Babuška and Cara;* 1991; *Crampin and Lovell*, 1991; *Savage*, 1999]. Thus the characterization of this property provides information about the stress/strain state. Upper crust anisotropy in the GoC region was first characterized in the Mexicali-Imperial Valley by *Zúñiga et al.* [1995] and *González and Munguía* [2003], who analyzed the birefringence that affects local S waves. Recently, the installation of broad band stations of the NARS-Baja and RESBAN arrays have enabled the first studies of the anisotropy of the crust and upper mantle throughout the entire region of GoC using surface waves [*Zhang et al.*, 2006; *Markee and Gaherty*, 2006; *Zhang et al.*, 2007] and also SKS waves [*Obrebski et al.*, 2006; *Van Benthem et al.*, 2006].

[5] Further information about the anisotropic structure of the lithosphere can be obtained through receiver functions (RFs) analysis, by forward modeling the anisotropic features observed on radial and transverse ground motion components [*Levin and Park*, 1998]. Possible evidences of anisotropy in receiver functions obtained at several NARS-Baja stations were reported earlier by *Persaud et al.* [2007], though they did not modeled them. Here we present possible forward models for the anisotropy of the shallow lithosphere beneath three stations located in the different tectonic provinces that comprise the northern/central GoC region and that show reasonable consistency with recent tectonic processes occurred in this area.

2. Data

[6] Receiver functions were calculated from teleseismic events recorded by the NARS-Baja array. Most stations have been recording since April 2002 and are equipped with three-component Streckeisen STS-2 broadband sensors [*Trampert et al.*, 2003]. In a previous analysis, *Obrebski et al.* [2006] found that the upper mantle under the region of study can be divided into five areas with distinct anisotropic patterns that appear to be fairly consistent with the characteristics of the structural provinces defined by *Stock et al.* [1991]. In this paper we analyzed data from the best stations representing each one of these provinces, namely, the stations with the lowest noise level and the longest database. We chose NE71 for the Transpeninsular Strike-Slip Province, NE75 for the Stable Central Peninsula and NE81 for the eastern Gulf Extensional Province (see Figure 1). Because stations NE71 and NE75 are located east of the former trench, they are of particular interest, since these stations allow us investigating possible oriented fabric frozen in the lithosphere and related to the fate of the Farallon Plate. The total area covered by our set of stations spans between 31.7N and 27.3N, and from 115.9W and 109.6W. We obtained good RFs from 82 events (see Table 1) recorded from April 2002 to June 2005. Focal depths of the earthquakes used range between 4 and 630 km, magnitudes from 5.6 to 8.5 and epicentral distances from 25° to 115°. Most of the teleseismic events used occurred in the South American subduction zone, around Fiji islands and in the northwestern and northern Pacific ring of fire (Figure 2). In contrast, the NE quadrant is poorly sampled.

3. Method

3.1. Receiver Functions

[7] Receiver functions are widely used to isolate and enhance information produced by lithospheric structures near the recording site such as velocity contrasts, dipping interfaces, sources of scattering and anisotropic layers. At teleseismic distances, this information makes up the first few seconds of the *P* waveform. Nevertheless, complex rupture history can introduce additional complexity in the direct *P* waves generating more than a single pulse. In addition, other compressive waves (*pP*, *PcP*) are often present. All those waves interact with the structure below the station generating redundant overlapped information. Teleseismic *P* phases propagate nearly vertically through the crust and thus the vertical component is typically little affected by the crustal structure. Under this condition, by deconvolving the vertical component from the horizontal ones, we eliminate the effects of the source rupture process and we obtain traces that are equivalent to those that we would observe from an incoming *P* waveform generated by a single pulse. We determined RFs following the method of *Ammon* [1991] that consists of calculating the ratio between horizontal (radial and transversal) and vertical components

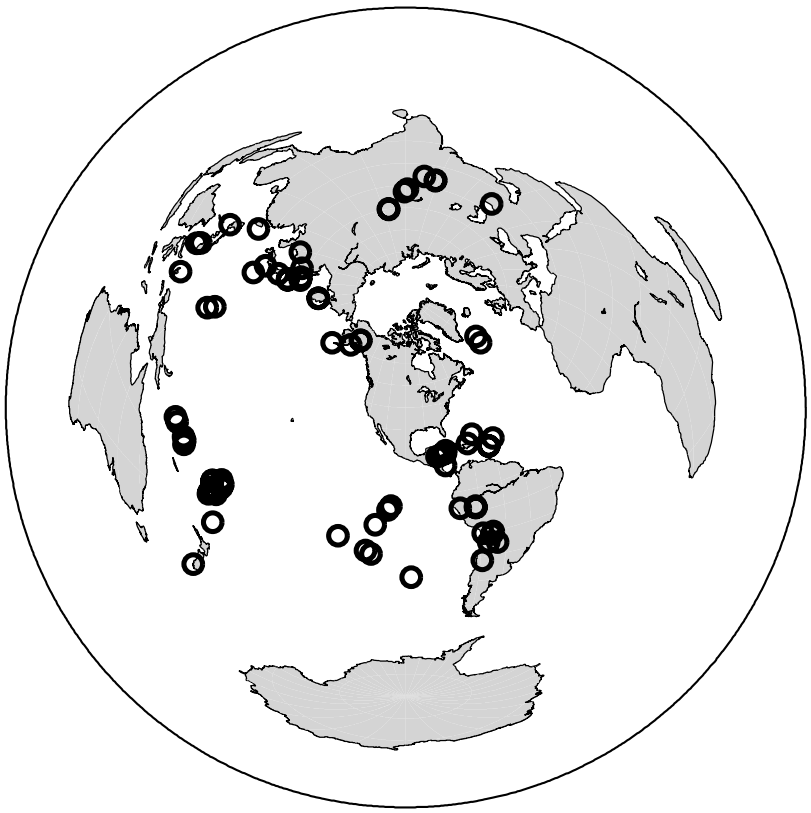

Figure 2. Distribution of the events used in this study. See Table 1 for detailed information about the seismic sources.

in the frequency domain. We selected seismic traces with clear *P* wave arrivals on both radial (R) and transverse (T) components.

[8] Time windows are 120 s wide and start 30 s before direct *P* first motion. Horizontal components are normalized by the vertical one. To achieve numeric stability, we use a "water level" of 0.001 to 0.01 [*Clayton and Wiggins*, 1976], and a Gaussian filter with width factor $a = 2$. Finally, RFs are smoothed applying a second-order zero phase Butterworth filter with a frequency band within 0.1–1 Hz. To enhance signal-to-noise ratio of the RFs in a particular direction, we sum single RFs in 20° wide azimuthal bins starting at 0–20° and so on. Only RFs with similar shape on R and T are stacked.

3.2. Main Potential Sources of Anomalous Transverse Energy

[9] Anisotropy [*Levin and Park*, 1998], dipping interfaces [*Langston*, 1977] and scattering produce anomalous energy on the transverse component. Each one of the features mentioned above controls the pattern of azimuthal variations of the *P wave* coda in a specific way so that the dominant source of the anomalous signal observed on the transverse component can theoretically been identified [*Levin and Park*, 1997; *Savage*, 1998]. Seismic anisotropy of the crust and upper mantle has been identified this way in different regions [*Levin et al.*, 2002a, 2002b; *Park et al.*, 2004; *Savage et al.*, 2007]. The azimuthal variations of the RFs obtained at NE71, NE75 and NE81 do not seem to be controlled by a dipping interface such as the Mohorovičić discontinuity (Moho) or by a source of scattering (see discussion below). Thus, we assume the anomalous transverse energy is mainly generated through the seismic anisotropy of the crust and upper mantle beneath these stations.

3.3. Characterization of the Seismic Anisotropy Through the Analysis of Shear Wave Splitting

[10] As a first step, we tried to characterize the crustal anisotropy assuming that the anomalous phases on T that seemed temporally coincident with the *P*-to-*S* converted phases at the Moho observed on R, arose from seismic birefringence in a single anisotropic layer confined to the crust. We made measurements of shear wave splitting following the technique proposed by *Silver and Chan* [1991]. This approach initially employed to retrieve upper mantle anisotropy was successfully extended by *McNamara and Owens* [1993] and further improved by *Peng and Humphreys* [1997] to study crustal anisotropy in northern Nevada. An example of shear wave splitting measurement performed at station NE75 is available in auxiliary material[1]. At stations NE71, NE75 and NE80 we obtained consistent measurements of shear wave splitting using individual RFs for events with similar back azimuth. Nevertheless, these results exhibit strong discrepancy when using events proceeding from different directions (the list of the estimations of the anisotropic parameters is also available in auxiliary

[1] Auxiliary materials are available in the HTML. doi:10.1029/2007JB005156.

Table 2. Preferred Anisotropic Velocity Models[a]

Layer	Thickness (km)	Vp (km/s)	Vs (km/s)	η	ϕ (deg)	θ (deg)	Density (kg/m^3)
			NE71				
C1	8	6.6 (−10%)	3.8 (−10%)	0.6	10	30	2800
C2	29	6.6	3.8				2800
M1	2	8	4.6				3400
M2	10	8 (+11%)	4.6 (+11%)	1	90	−45	3400
M3	12	8 (+11%)	4.6 (+11%)	1	110	−20	3400
M4	∞	8	4.6				3400
			NE75				
C1	26	6.6	3.8				2800
C2	4	6.6 (−10%)	3.8 (−10%)	0.5	45	−45	2800
M1	4	8	4.6				3400
M2	6	7.1 (−15%)	3.8 (−15%)	0.5	45	50	3000
M3	∞	8	4.6				3400
			NE81				
C1	11	5.8	3.2				2600
C2	2.5	5.8 (−10%)	3.2 (−10%)	0.5	60	45	2600
C3	3.5	5.8 (−10%)	3.2 (−10%)	0.5	150	45	2600
C4	8	5.8	3.2				2600
M1	∞	8.1	4.6				3400
			NE81, Alternative Model				
C1	3	4.5	2.5				2210
C2	1	5.8	3.2				2600
C3	3	5.8 (−10%)	3.2 (−10%)	0.5	200	30	2600
C4	3	5.8 (−10%)	3.2 (−10%)	0.5	260	30	2600
C5	14	5.8	3.2				2600
M1	∞	8.1	4.6				3400

[a]C refers to crust layers, and M refers to mantle layers. Percentage of anisotropy is given in parentheses. Positive (negative) percentage indicates the symmetry axis is fast (slow). Parameter η controls the distortion of the quasi-ellipsoids with which velocities are described in hexagonal anisotropic medium. Parameter ϕ is the azimuth of the symmetry axis, and θ is its dip measured from horizontal direction and positive up. In the case of NE81, an alternative model is also shown (Figure 7).

material). This azimuthal dependency is more complex than π or $\pi/2$ periodicity and therefore cannot be accounted for with simple crustal models having one anisotropic layer with a particular dipping fast axis or a stack of two anisotropic layers with distinct axis directions [*Silver and Savage*, 1994]. In addition, the time delays that we obtained were far too large compared with those obtained for the crust in other regions. Thus, we conclude that our initial assumption of anomalous phases on the transverse component resulting from the birefringence of the *P*-to-*S* converted phase in a single anisotropic layer located within the crust cannot account for the anisotropic features observed in the RFs that we obtained at NE71, NE75 and NE81.

3.4. Forward Modeling of the Receiver Functions Waveforms

[11] An alternative approach to resolve less restrictive anisotropic models of the upper lithosphere is by modeling directly the RFs waveforms. Because of the large number of parameters, direct modeling of the RFs [*Savage*, 1998; *Savage et al.*, 2007; *Levin et al.*, 2002a, 2002b] is typically performed rather than a rigorous inversion [*Levin and Park*, 1997]. For this reason the models presented here are intrinsically likely to be nonunique. Thus, as a criterion, we favor models which are consistent with the geologic and tectonic settings apart from allowing a good fit of the real data. Other limitation of our study is that the RFs are not well constrained in some azimuthal ranges (see section 2), either because large teleseismic events are simply not available such as the northeastern quadrant, or because the RFs display a low signal-to-noise ratio, especially on the transverse component. Under these conditions, the models discussed in this paper cannot be fully constrained. The RFs are fitted using synthetic seismograms. For that purpose, we wrote a reflectivity code based on *Keith and Crampin* [1977a, 1977b, 1977c] and *Park* [1996]. With the intention of reducing the number of model parameters, we only considered models with anisotropic layers displaying hexagonal symmetry. This symmetry system is among the simplest, but as shown in previous studies [*Savage*, 1998; *Park et al.*, 2004] it describes with good fidelity the anisotropic characteristics of the rocks in the crust and upper mantle. Our code allows the slow or fast symmetry axis to dip in any direction, but it does not consider plunging interfaces. We calculated the stiffness tensors following *Farra et al.* [1991]. For hexagonal symmetry, the stiffness tensor is fully described by 5 independent coefficients that can be related to the mean compressional and shear wave velocities, the percentage of anisotropy for both type of waves and the parameter η that describes the distortion of the velocity ellipse. We gave the same percentage of anisotropy to both wave types. For each azimuthal bin, we generated individual synthetic seismograms with the same angles of incidence and back azimuth, as the real data. Synthetic seismograms then undergo the same processing as real data to obtain synthetic receiver functions that we stack to obtain the synthetic RFs showed in Figures 4 to 7. Thus, synthetic and observed RFs can be directly compared with the observations.

[12] Because no detailed isotropic velocity models have been calculated so far for the crust under the stations NE71, NE75, and NE81, we used models obtained in close areas as initial velocity model. Thus, we have no a priori idea of the detailed structure of the crust beneath stations NE71, NE75 and NE81. Therefore, we do not pretend to match our synthetic RFs perfectly with the real ones. We rather aim to find models that conceptually capture the azimuthal variation of the prominent features and that are consistent with the geologic and tectonic features of the area under study. We adopted the following approach: First, we isolate prominent phases. No attention is paid to wiggles that are not coherently observed in a wide azimuthal range. As explained above, the detailed structure of the crust is not known. For this reason, isolated wiggles may result from localized source of scattering. They may also simply represent residual noise after stacking, especially when the stacked RFs are calculated from very few individual RFs. We then fix the Moho depth using the most prominent *P*-to-*S* conversion on the radial components. We prefer not to take into consideration low-velocity superficial layers. Since attenuation is not taken into account when we calculate the synthetics, the amplitudes of the reflections generated in low-velocity layers are overestimated and may affect later phases. The second step is to introduce anisotropy in order to match the transverse components where the effects of anisotropy are generally stronger and more evident, but we also take into consideration the radial anisotropic features. We focus on changes of polarity and amplitude with azimuth. A strong trade off exists between the percentage of anisotropy, the parameter η and the inclination of the symmetry axis, since these three parameters control the amplitude of the anisotropic phases. In order to reduce the number of free parameters, we made $\eta = 0.5$ for the crust, a typical value for highly anisotropic crustal rocks [*Godfrey et al.*, 2000] and $\eta = 1$ for mantle rocks [*Farra et al.*, 1991].

4. Results

[13] In this section we describe the main features of the RFs obtained (Figures 4 to 7) and the reasoning that guided us to resolve possible anisotropic models at each particular station. The transverse signal-to-noise ratio at 2 s ranges from 1 to 100 for the 39 observed stacked RFs obtained at station NE71, NE75 and NE80. The mean value is 18.7 and only in five cases the SNR is inferior than 2. These cases correspond to stacked RFs obtained from very few individual RFs. We set the time $t = 0$ to correspond with the maximum amplitude of direct *P* wave arrivals. We will refer to ''one-sided'' pulse to describe the shape of a phase composed of one single swing. A one-sided pulse with upward first motion will be called ''positive'' one-sided pulse. We will also use the term ''two-sided'' and ''three-sided'' pulse to refer to a sequence composed of two or three pulses with alternating polarities. A positive swing immediately followed by a negative one will be referred to as ''positive-negative'' two-sided pulse and so on. We employ ''zero delay'' to describe any phase that appears on the transverse component and that is temporally coincident with direct *P* wave on the radial component. The stacked RFs are referred to on the basis of their back azimuthal range (using stacking bins from 0°–20° to 340°–360°). To describe the range over which a certain feature is seen, we indicate the lower and upper limit of the first and last back azimuthal bins respectively, that display this feature. For example, if we report certain feature that appears between 80° and 140° it means it is seen continuously on the stacked RFs that correspond to the bins 80°–100°, 100°–120° and 120°–140°. The symmetry axis in each anisotropic layer of our models is defined by its azimuth ϕ measured positively clockwise from north and its dip θ measured from horizontal direction and positive upward. We depict the azimuthal pattern of one particular phase on T as ''two-lobed'' or ''four-lobed'' depending on the number of directions at which the polarity of the phase switches (one or two, respectively). The descriptions of the models referred to in this section are all listed in Table 2 (see also Figure 3).

4.1. Transpeninsular Strike-Slip Province: Station NE71

[14] We observe a large positive one-sided pulse on R that arrives 4.4 s after the direct *P* wave (Figure 4), and we interpreted that pulse as the *P*-to-*S* converted wave at the Moho (Ps_{Moho} hereafter). It is best seen in the back azimuthal range 180°–360°. It yields maximum amplitude toward 280°–300° and apparently weakens around 80°–100° and 120°–140°. The arrival time of this phase does not change with azimuth. The transverse components exhibit two main features. A zero delay two-sided phase switches polarity between 140° and 240°. It is followed by a two-sided pulse that arrives approximately at same time as Ps_{Moho} and displays a reversal of polarity between 260° and 280°. The second swing of this two-sided pulse is markedly broader than the first.

[15] As a starting point, we use the isotropic velocity model of *Nava and Brune* [1982] (hereafter referred to as NB82). Since the RFs do not exhibit any clear and coherent pulse between direct *P* wave and Ps_{Moho} on R, we cannot resolve any conspicuous middle crust velocity contrast. Thus, we consider a homogeneous crust with the same characteristics as those of the middle crust layer of the NB82 model, i.e., with $V_P = 6.6$ km/s (see Table 2). The broad zero delay phase on T is matched by introducing a thick anisotropic layer C1 immediately beneath the free surface. The polarity reversal of this phase on T permits us to constrain the axis of symmetry to have an azimuth $\phi = 10°$. The two-lobed pattern also implies that the axis of symmetry cannot be horizontal [*Savage*, 1998]. Dipping the symmetry axis 30° from the horizontal, the model captures the amplitude variations with azimuth with fidelity. The arrival time of the second two-sided pulse on T indicates that the anisotropic layer that generated it is below the Moho (M2 in Table 2). Actually, a thin isotropic layer M1 (see Table 2) below the crust is also required for the pulses generated in M2 to coincide temporally with that observed on the data. The two-lobed pattern indicates that the symmetry axis in M2 dips. Because of the lack of sharpness of both Ps_{Moho} on R and the two-sided pulse on T between 0° and 180°, the value of its inclination cannot be well resolved, so we fix it at 45°. This way, synthetic waveforms on R and T show minimum amplitude between 0° and 180°. The approximately E-W fast axis of symmetry accounts for the change of polarity on T and give rise to the increase of

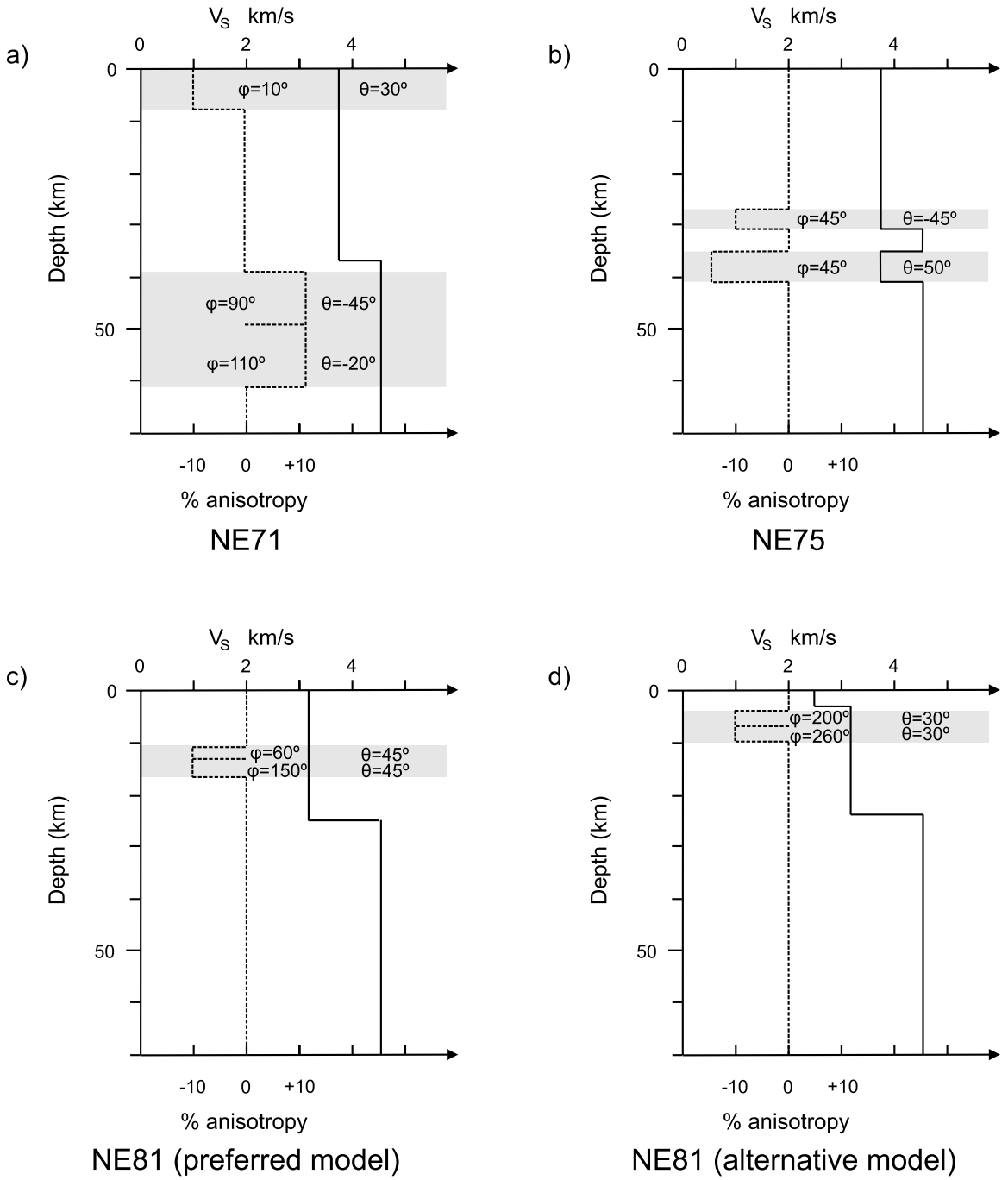

Figure 3. Vertical profile of our preferred anisotropic velocity models resolved at the three stations (also described in Table 2): (a) NE71, (b) NE75, and (c) NE81. (d) An alternative model for NE81. The black line represents the average *S* wave velocity, and the dotted line indicates the percentage of anisotropy. Shaded areas highlight anisotropic zones. In each anisotropic layer, "ϕ" and "θ" are the azimuth of the axis of symmetry and its dip, respectively, which is positive upward.

Ps_{Moho} amplitude observed on the radial component toward west. Introducing a third anisotropic layer M3 beneath M2, we manage to broaden the second swing of the two-sided pulse. Introducing a 1 km thick isotropic layer between M2 and M3 greatly improves the fit (not shown). *Owens* [1987] suggests that at 1 Hz, RF analysis allow for resolving features as thin as 1 km. Nevertheless, such thin isotropic layer has no straightforward geologic explanation thus we chose not to include it.

4.2. Stable Central Peninsula: Station NE75

[16] The RFs on R show a clear positive pulse at 3.4 s that we interpret as Ps_{Moho}, the Moho *P*-to-*S* converted phase (Figure 5). The Ps_{Moho}-to-*P* amplitude ratio displays substantial azimuthal variation and reaches its maximum to-

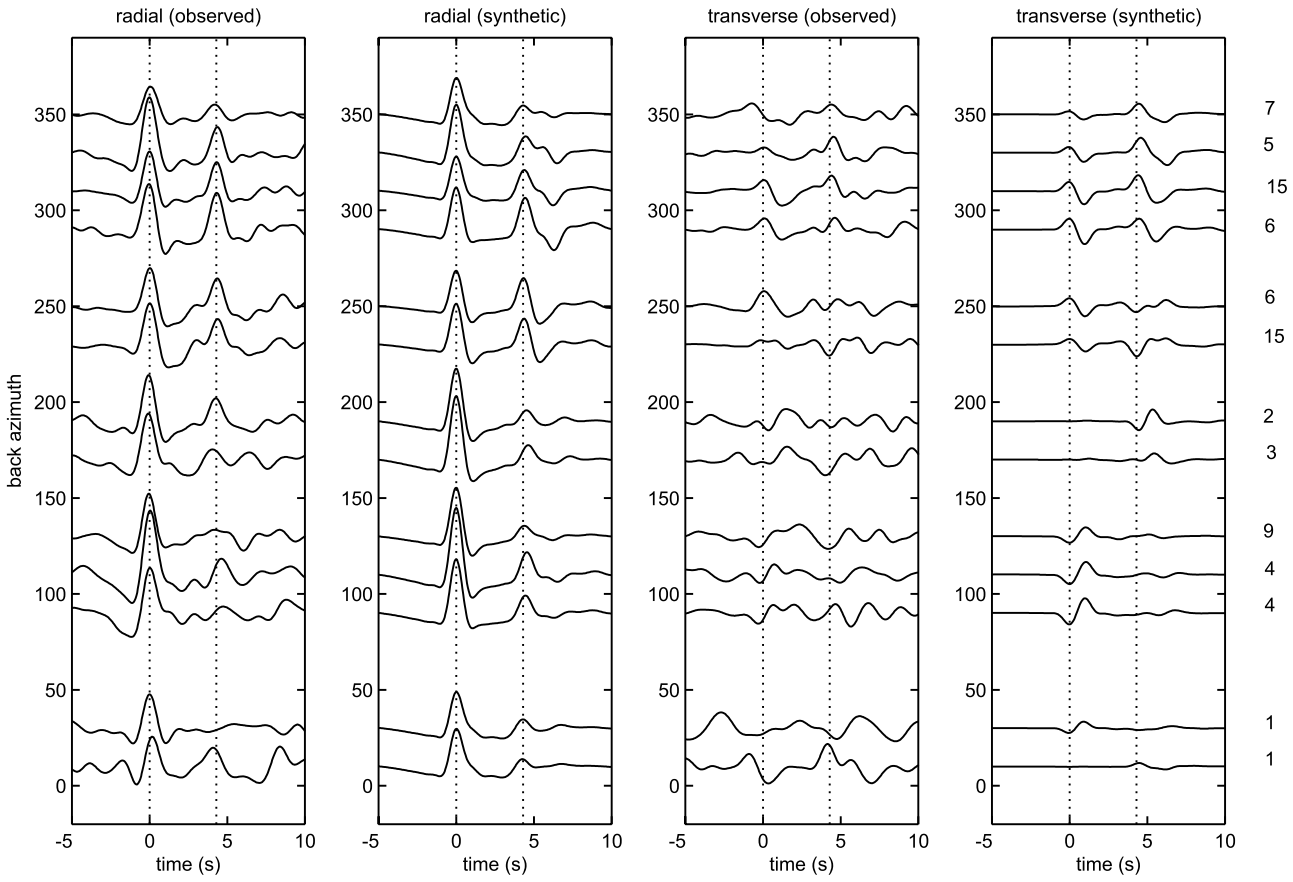

Figure 4. Azimuthal pattern of observed and synthetic receiver functions at station NE71. The number of individual RFs stacked in each 20° wide bin is listed on the right. Vertical dotted lines indicate the arrival of direct *P* phase and the phase that we interpret as the *P*-to-*S* conversion at the Moho. The parameters of the preferred model used are listed in Table 2.

ward WSW (220°–260°). In the back azimuthal ranges 0–100° and 340°–360°, Ps_{Moho} arrives somewhat earlier and in the back azimuthal range 0°–100° it is followed by another large positive pulse that we call *Ps*'. On T, the most prominent feature is a large three-sided pulse, which displays a clear polarity switch between 20° and 80°.

[17] As for station NE71 we use the middle layer of the NB82 model as the isotropic starting model (see Table 2). The first swing and part of the second swing that compose the three-sided pulse on T are generated by a conversion in an anisotropic layer located in the base of the crust (C2 in Table 2). A reasonable fit is achieved giving the symmetry axis an azimuth $\phi = 45°$ and a dip $\theta = -45°$. Nevertheless, a second layer (M2 in Table 2) is required to satisfy the larger amplitude of the central swing and to generate the third one. To adequately match time arrivals this second layer is constrained to be in the mantle, a few kilometers beneath the continental Moho. Anisotropic rocks in the mantle are typically but not always best described with a fast symmetry axis [*Zhang and Karato*, 1995; *Jung and Karato*, 2001]; thus we first tried to match the data by giving to M2 a fast axis of symmetry. Nonetheless, using this model, the maximum of Ps_{Moho} on R and that of the three-sided pulse on T are observed for the same azimuthal range, in disagreement with the data, unless the symmetry axis has a nearly vertical inclination. Using such dip to satisfy the large amplitude of the phases on T, we must increase the percentage of anisotropy at a level clearly not pertinent for typical mantle aggregates. Alternatively, we tried to give a slow axis of symmetry to M2 rather than a fast one. This way the azimuthal patterns of variation on both radial and transverse components are reasonably modeled. Furthermore, the anisotropic characteristics of M2 cause the amplitude of *Ps*' to be modulated in such a way it is observed only in a small back azimuthal range, in agreement with the data.

[18] The large one-sided negative pulse that follows immediately the direct *P* wave on R (see Figure 5) can be generated introducing a very low velocity zone beneath the free surface. Nonetheless, this layer also generates a large reflection on R after Ps_{Moho} that is not observed in real data (time arrival different from that of *Ps*'). This feature will probably be much weaker if attenuation were taken into account in the synthetic calculations. Since it is not the case, we decided not to include this layer in our model. Nevertheless it is worth reporting that when we tried to introduce such low-velocity layer, it gave rise to reflections on T that significantly contributed to the amplitude of the first two swings that compose the three-sided pulse. This implies that

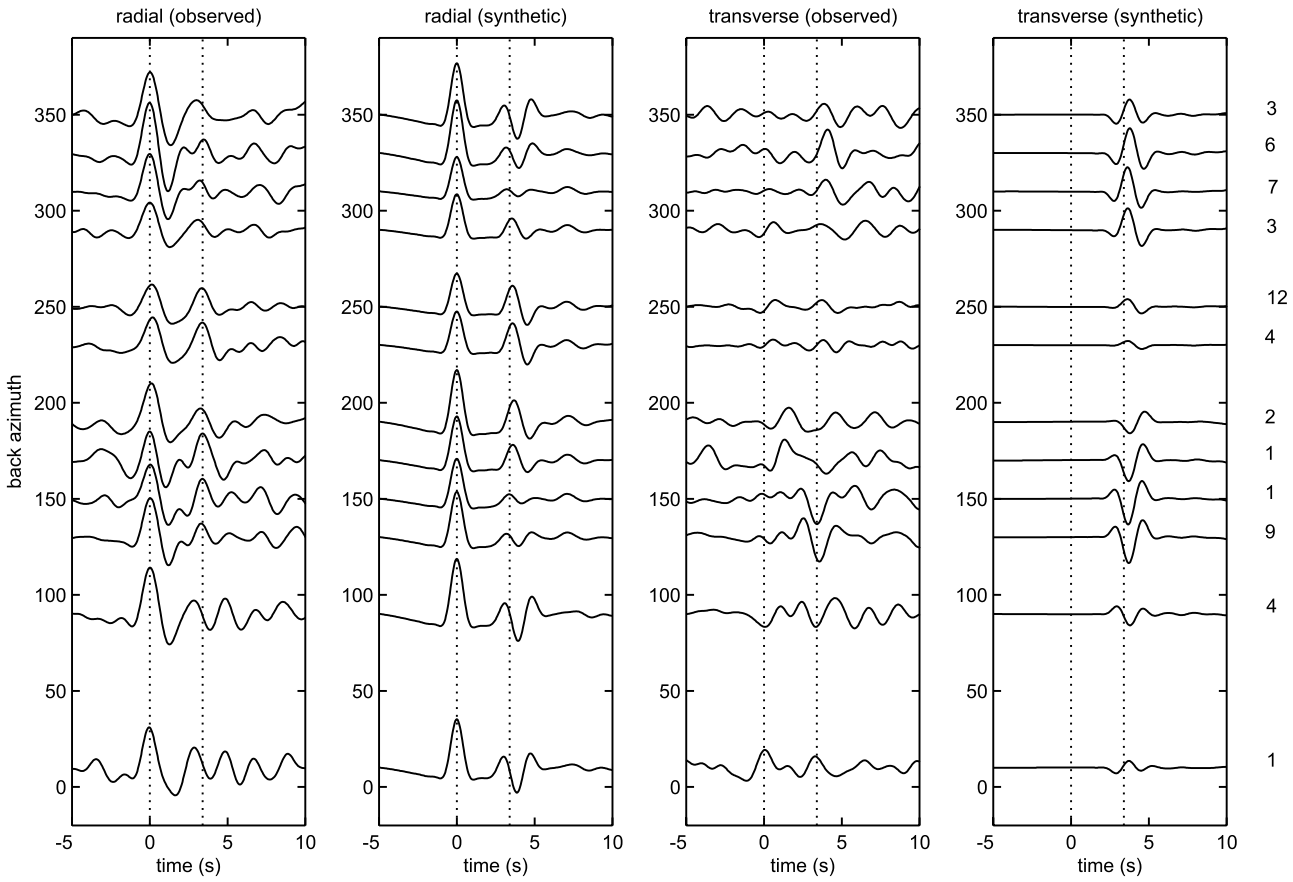

Figure 5. Same as Figure 4 but for station NE75. The synthetic receiver functions were obtained with our preferred model described in Table 2.

omitting the contribution of the surface low-velocity layer leads us to overestimate the percentage of anisotropy in C2.

4.3. Eastern Gulf Extensional Province: Station NE81

[19] Figure 6 shows the observed and synthetic RFs obtained for station NE81. For back azimuths in the range 0°–60° and 160°–360°, the radial components show a two-sided positive-negative pulse between 1 and 3 s. The delay time of this pulse, with respect to the direct *P* wave, increases slightly with increasing azimuth. Then, a large positive pulse arrives consistently at 3.8 s in all directions. We interpret this last pulse as the *P*-to-*S* conversion at Moho (Ps_{Moho}). On T a sequence of two positive pulses are clearly seen between 1 and 4 s for back azimuths in the range 0–60° and then 240°–360°. The amplitude of the first pulse becomes continuously larger from 240° to 360° and from 0° to 60° and the amplitude of the second pulse displays inverse variation with increasing back azimuth. These two pulses arrive progressively later as back azimuth increases, and no clear π periodic polarity reversal can be observed. These variations exhibit a rather "corkscrew" pattern [*Park et al.*, 2004]. Finally, the transverse component vanishes between 80° and 120° and then between 160° and 200°.

[20] We used as initial isotropic velocity model that proposed by *Harder and Keller* [2000] (hereafter referred to as HK02) obtained using data from a seismic profile deployed in New Mexico, close to the Mexico-U.S. international border. Aside from the large two-sided positive-negative pulse observed on R, we cannot resolve any phase that suggests a conspicuous velocity contrast within the crust. A good fit for the Ps_{Moho}-to-*P* amplitude ratio is achieved by considering as a starting isotropic model a homogeneous crust with a quite low *P* wave velocity of 5.8 pkm/s (corresponding to the middle layer of the HK02 model). We also tried to include an additional faster layer in the lower crust as in the HK02 model, but in this case the Ps_{Moho}-to-*P* amplitude ratio markedly drops. Typical seismic velocities in the lower crust are larger than 6 km/s suggesting that our model is too simplistic. A more detailed analysis of the velocity of both crust and upper mantle beneath NE81 could shed light on the reason of the large Ps_{Moho}-to-*P* amplitude ratio observed at the Moho discontinuity beneath this station but such analysis is beyond the scope of this study. The anisotropic features described above cannot be satisfied using separate single anisotropic layers since such models yield clear π periodic or $\pi/2$ periodic polarity reversals on T. Furthermore they generally give rise on T to rapid azimuthal variations in amplitude. On the other hand, a stack of two anisotropic layers generates a pattern consistent with what we observe at NE81. In particular, we find that a stack of two anisotropic layers in the middle crust that have dipping symmetry axis with perpendicular azimuth satisfies both radial and transverse pattern (Figure 6). On R, the large two-sided positive-

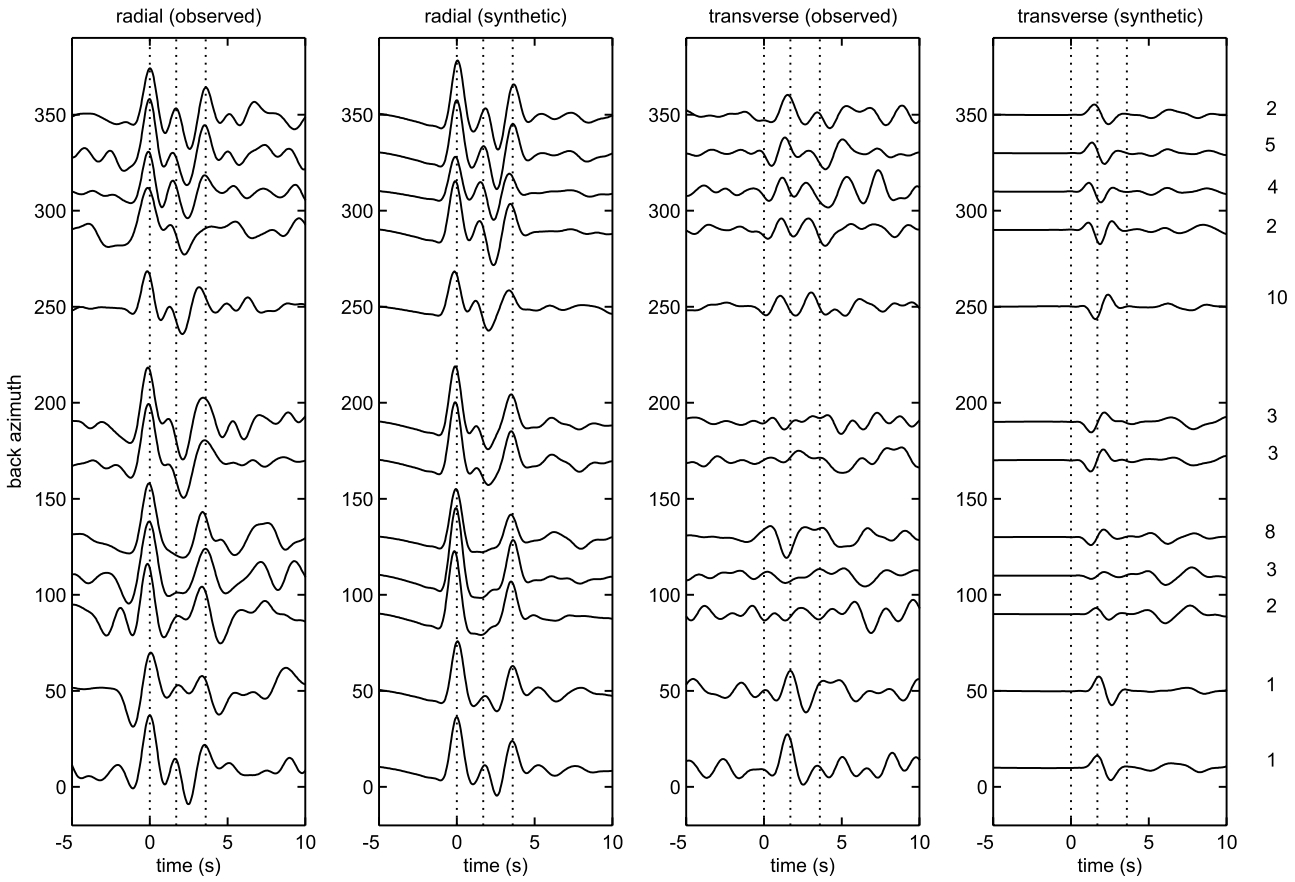

Figure 6. Same as Figure 4 but for station NE81. The synthetic receiver functions were obtained with our preferred model described in Table 2.

negative pulse between the direct *P* and the converted Ps_{Moho} waves is generated by the stack of two layers and vanishes toward ESE (80°–120°). On T, the shape of the two individual pulses that compose the sequence depicted above is not well matched. However, the main trends of their back azimuthal variation are captured with good fidelity: the amplitude of each pulse does not exhibit rapid variation with back azimuth, their arrival times slowly increase clockwise, and a gradual energy transfer from the first to the second pulse is observed, in agreement with the data. Finally, the amplitude of both pulses clearly decreases between 80° and 120° though not between 160° and 200°. We also tried an alternative model that is made of a superficial low-velocity layer C1 atop a stack of two anisotropic layers C3–C4 (see Table 2 and Figure 7). On R, the large two-sided positive-negative pulse between direct *P* wave and Ps_{Moho} can be explained as reflections generated in the low-velocity layer beneath the free surface. The combined effects of anisotropic conversions in this stack C3–C4 on one hand and reflections in uppermost low-velocity crust on the other hand reproduce the two pulses on T comparatively better than the first model. However, using this second model, the shape of both radial and transverse components toward ESE (80°–120°) is not so well matched. Thus we regard the first model as the best one. The study of the second model showed that the knowledge of slight velocity contrast would enable us to generate reflections that may improve the fit of the first model.

5. Discussion

5.1. Alternative Explanation for Anomalous Energy on the Transverse Component

[21] As mentioned above, possible sources of transverse energy other than seismic anisotropy may exist. One of these is the inclination of the Moho which we can discard with certain confidence, because the *P* and Ps_{Moho} would both show energy on the transverse component with similar amplitude but opposing polarity [*Cassidy*, 1992; *Savage*, 1998; *Levin and Park;* 1998]. At NE75 and NE81, the direct *P* wave does not yield any conspicuous transverse component in a wide range of azimuths and at NE71 the directions of polarity reversal of the *P* and Ps_{Moho} on T are different. Thus the Moho must be roughly horizontal beneath these stations. In addition, if the Moho had a significant dip, the Ps_{Moho} would display a clear and simple azimuthal moveout which is not the case at least for NE71 and NE81. These conclusions are in agreement with those of *Persaud et al.* [2007], who did not report significant Moho dip for NE71 and only shallow dip beneath NE75, the direction of which (S-SE) is moreover clearly inconsistent with that of the polarity switch of the transverse anomalous phases we reported for this station.

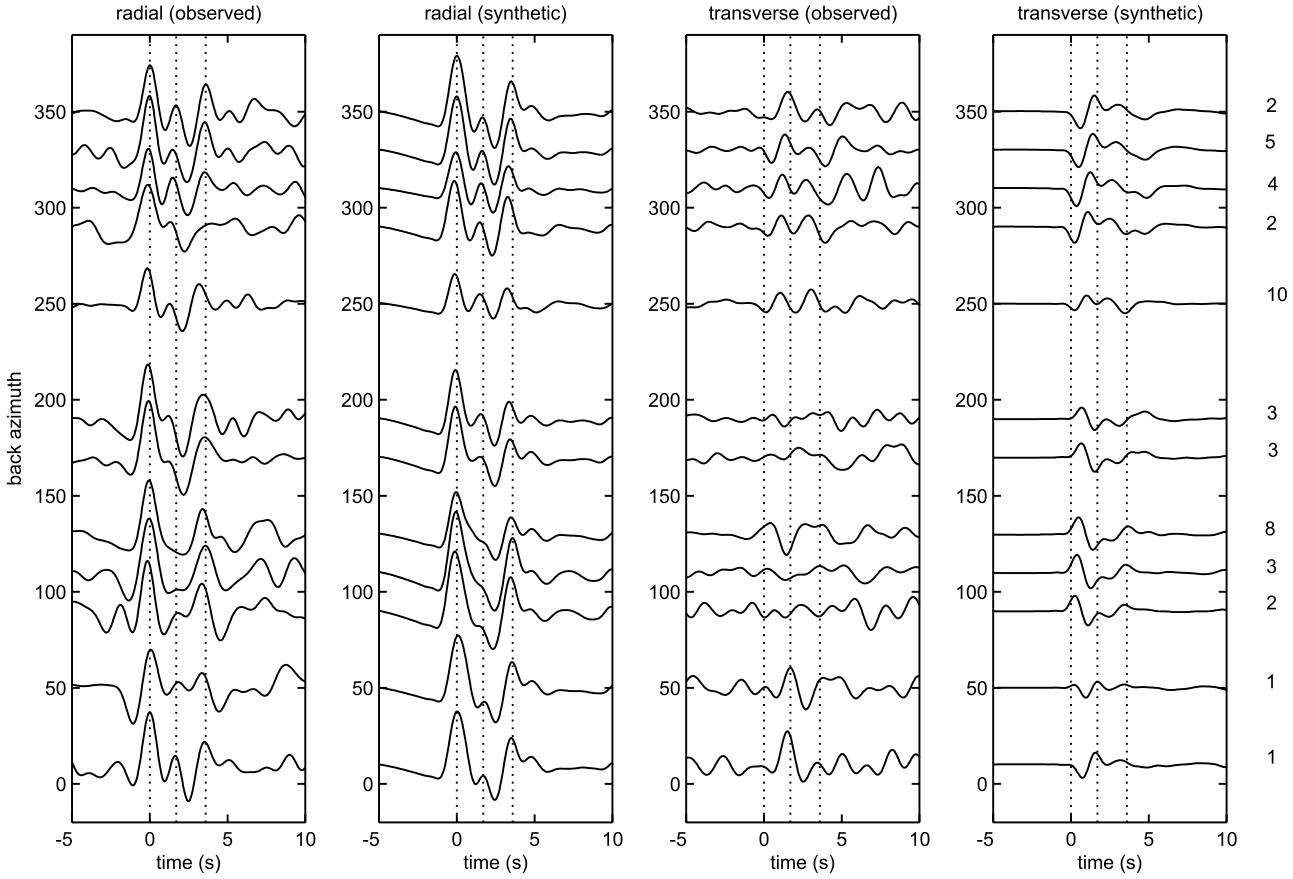

Figure 7. Same as Figure 6 but with the synthetic receiver functions calculated on the basis of an alternative model whose characteristics are available in Table 2.

[22] Another possible source of energy observed in the transverse ground motion component is a localized source of scattering below the recording stations. However, we can also discard this possible source of transverse energy because scattered waves are generally independent of azimuth [*Aki*, 1973] and the amplitudes show large random spatial variations. In contrast, the RFs obtained in our analysis exhibit smooth and coherent variations between close azimuthal bins. In addition, if the energy arriving after *P* and recorded in the transverse component were due to scattered *P* waves, then the particle motion would be consistent with that expected for *P* waves. This is not the case since at each station we observe Ps_{Moho} waves with elliptical particle motion (see the auxiliary material), whereas the arrival of the direct *P* wave is typically lineally polarized along the radial component.

5.2. Transpeninsular Strike-Slip Province: Station NE71

[23] Anisotropy in the upper crust is typically controlled by preferential alignment of cracks either by regional state of stress or by a nearby fault system, and displays a slow axis of symmetry normal to the cracks plane [*Crampin and Lovell*, 1991; *Cochran et al.*, 2006]. N-S slow symmetry axis is consistent neither with N-S regional maximum horizontal stress nor with NW-SE trend of the close San Miguel strike-slip fault system. On the other hand, the roughly E-W rock foliation reported by *Gastil et al.* [1975] in batholithic outcrops near station NE71 seems a more pertinent explanation.

[24] The lack of anisotropy in layer M1 of our model (Table 2) may indicate the absence of deformation in the strong dunite rocks beneath the lower crust-upper mantle boundary. Alternatively, M1 might be a transition zone where fabric is not coherent enough to generate strong anisotropy.

[25] The nearly E-W fast symmetry axis in the mantle anisotropic layers M2 and M3 of our preferred model is similar to the roughly E-W fast direction in the upper mantle reported along most of the former trench [*Özalaybey and Savage*, 1995; *Polet and Kanamori*, 2002] in western North American plate and along the northern half of the Baja California Peninsula [*Obrebski et al.*, 2006; *Zhang et al.*, 2007] though the fast direction estimated from SKS waves is rather oriented WSW-ENE beneath NE71 [*Obrebski et al.*, 2006]. As proposed by *Özalaybey and Savage* [1995] for the case of the North American borderland in California, the upper mantle fabric responsible for the E-W fast axis beneath the Baja California Peninsula may be controlled by the opening of a slab window and the eastward motion of the sinking fragments of the Farallon Plate, or by past ~E-W thrust during Farallon flat subduction [*Atwater*, 1989]. The velocity models of *Zhang et al.* [2007] are suggestive of slower and possibly hotter mantle beneath the site of NE71, in consistency with the asthenospheric window hypothesis.

Nevertheless, the geographic coincidence of a slab window with the mechanically strong, roughly unextended crust of the Baja California Peninsula is questionable, as discussed by *Fletcher et al.* [2007]. In the southern Sierra Nevada, *Zandt et al.* [2004] imaged a peculiar lithospheric structure that they interpreted as due to the possible foundering of the dense lithospheric root of the former arc. *Yang and Forsyth* [2006] highlighted in southern California a similar lithospheric structure suggesting that part of the former arc may have also foundered in this area and perhaps farther south. So far, this hypothesis has not been verified. Thus we can only speculate that the eastward dipping fast symmetry axis in the layers M2 and M3 might be linked to downward west-to-east flow indicating that the space left by the dripping lithospheric root would be centered east of NE71, in the Gulf Extensional Province.

5.3. Stable Central Peninsula: Station NE75

[26] The NE-SW slow symmetry axis resolved in both anisotropic layers of our model is in good agreement with the NW-SE fast direction estimated by *Zhang et al.* [2007] for the lithosphere beneath this station.

[27] The shallower anisotropic layer C2 lies at the base of the crust. Anisotropy may arise from preferential alignment of either intrinsically anisotropic minerals or melt filled cracks. Supposing this pattern is due to a well developed shear zone, these two sources imply opposite sense of shear. The first possibility could be interpreted as the result of flow in the lower crust toward the GoC, possibly triggered by the onset of rifting in the Gulf Extensional Province. These flows would explain the gulfward thinning of the crust reported previously along the Baja California Peninsula [*López-Pineda et al.*, 2007; *Persaud et al.*, 2007] and possibly the absence of new seafloor spreading along several segments of the oblique rift within the GoC, in spite of the intense extension that has taken place there since middle Miocene [*Lewis et al.*, 2001; *Persaud et al.*, 2007]. Nevertheless, NE75 is located west from the Guaymas Basin where a large amount of new oceanic crust has been documented [*Aragón-Arreola et al.*, 2005] so that the existence of significant gulfward flows in the lower crust beneath NE75 are questionable. Alternatively, the preferential orientation of melt filled cracks is also convincing since this implies a sense of shear which is consistent with the past thrusting direction. Moreover, the presence of melt was probable due to the prevalent subduction conditions until middle Miocene.

[28] An intriguing feature of our preferred model is that the deeper anisotropic layer displays a slow symmetry axis rather than a fast one, as observed in most mantle rocks. Station NE75 is located about a hundred kilometers east from the former Farallon-North American trench. Thus the anisotropic layer M2 could correspond to a fragment of stalled and strained oceanic crust or to material from the mantle wedge metamorphosed through the shear and the dehydration of the slab associated with the subduction conditions. In both cases, the anisotropy is likely to result from the preferred orientation of hydrous minerals and thus a slow axis of symmetry is expected [*Savage*, 1998; *Park et al.*, 2004]. To obtain our best fitting model (Figure 5 and Table 2), we gave to the anisotropic layer M2 seismic velocities (V_P = 7.1 km/s, V_S = 3.8 km/s) and density (ρ = 3000 kg/m^3) typical for oceanic crust. This way, the moderate velocity contrast at its deeper interface generates a conversion seen on R with arrival time consistent with that of *Ps*' (see Figure 5). We also tested an alternative model similar to that of *Park et al.* [2004], in which the anisotropy results from a layer of mantle metamorphosed to serpentine because of subduction conditions. Serpentine is highly anisotropic and has a density around 2600 kg/m^3 far lower than that of the upper mantle material. Nevertheless, when we include an anisotropic layer with such low density in our model, the strong velocity contrasts at its upper and lower interfaces generate phases on R larger than that really observed on the data. The effect of anisotropy is not strong enough to compensate these pulses. We cannot increase the percentage of anisotropy in M2 since this way the amplitude of the three-sided pulse on T would not be fitted any more. *Ps*' is therefore observed in all directions, which is not the case in the data. Thus the characteristics of M2 appear to be rather consistent with that of oceanic crust than that of completely metamorphosed mantle wedge. *Bohannon and Parsons* [1995] proposed that, because of their buoyancy, most of the fragments of the Farallon slab may have stalled beneath the North American borderland after the cease of the subduction. Our model may represent one of the few evidences of the presence of these fragments beneath the Baja California Peninsula, together with the resistivity model obtained by *Romo* [2002]. His model revealed a flat highly conductive anomaly across the peninsula, at about parallel 28°N (just a 100 km northwest of NE75), interpreted as a suture zone between the Baja Peninsula crust and the Guadalupe plate.

[29] Finally, it is encouraging to note that the location and nature of the two anisotropic zones in our model are in agreement with the mechanical model developed by *Bohannon and Parsons* [1995, Figure 13.E] that predicts two weak zones around the Moho in the borderland, one in the lowermost crust of the peninsula and another one that corresponds to the remnants of the slab stalled beneath the continental lithosphere. Further, in the strength model obtained by these authors, these two weak layers are separated by a comparatively stronger mantle layer of dunite that roughly corresponds to layer M1 in our anisotropic model (see Table 2). In view of these vertical variations in rock strength, it is unlikely that strain was concentrated in the strong dunite layer and this may explain the absence of anisotropy in the layer M1 of our model.

5.4. Structural Contrasts Along the Baja California Peninsula

[30] The anisotropic models obtained at NE71 and NE75 are quite different despite both stations are located on the Baja California Peninsula. Beneath NE75 in the central peninsula, the anisotropy in the first kilometers of the mantle is consistent with the presence of either deformed oceanic crust or material of the metamorphosed mantle wedge. As discussed above, the lower continental crust beneath NE75 also seems to have registered the effects of shear associated to the subduction of the Farallon slab. Thus, the model obtained suggests that the Farallon plate was subducting shallowly beneath the site of NE75. In contrast, the model obtained at NE71 in the northern part of the peninsula does not require any anisotropic layer in the

lower crust, and the anisotropic zone in the first 25 km of the mantle is not suggestive of the presence of either oceanic crust or metamorphosed wedge that would unambiguously mark the top boundary of a stalled oceanic slab. Effectively, the layers M2 and M3 beneath NE71 display characteristics consistent with that of typical anisotropic mantle rocks, i.e., which exhibit a fast symmetry axis. In addition, no conspicuous radial pulse following Ps_{Moho} is observed in the RFs; thus the presence of material with density significantly inferior than that of the mantle is unlikely, at least in the first 25 km of the mantle.

[31] *Zhang et al.* [2007] also imaged a sharp contrast in upper mantle seismic waves velocities between the northern and central southern parts of the Baja California Peninsula. Their models show fast anomalies that may be interpreted as possible remnants of the Farallon slab. Beneath the central/southern part of the peninsula, including the site of NE75, the fast anomaly appears to lie just beneath the continental crust. In contrast, the fast anomaly is markedly deeper to the north. This geometry of the remnants of the slab suggested by the velocity model of *Zhang et al.* [2007] could explain why the anisotropy of the shallow lithosphere seems to be associated to the slab-mantle wedge interface beneath NE75 but not beneath NE71, since in this case the top of the slab may lie deeper than 65 km, the lower limit of our model.

[32] As suggested by other authors [*Stock and Hodges*, 1989; *Gans*, 1997; *Dorsey et al.*, 2006], the capture by the peninsula of fragment of the Farallon slab mechanically linked to the Pacific Plate may carry relevant implications for the reorganization of the plate boundary after the cease of subduction. In particular, the discrepancy in the geometry of the fragments of the slab along the peninsula suggested by the velocity model of *Zhang et al.* [2007] and by our own study may be correlated with the structural variations documented along the axis of the plate boundary within the GoC [*Dorsey et al.*, 2006] which constitutes an important but poorly understood feature of this oblique rift.

5.5. Eastern Gulf Extensional Province: Station NE81

[33] Our preferred model is consistent with a stack of two thin anisotropic layers in the intermediate crust (Figure 6 and Table 2). We have to keep in mind that using a model that includes anisotropic layers stacked rather than spatially separated, the estimation of the parameters that define the symmetry axes are typically far less constrained. None of the symmetry axes seems correlated to today's roughly E-W direction of extension reported in this area [*Suter and Contreras*, 2002]. On the contrary, the WSW-ENE slow axis in the stack's upper layer is similar to the SW-NE to WSW-ENE Basin-and-Range extension that occurred in the eastern Gulf Extensional Province chiefly from late Oligocene to middle Miocene time [*Gans*, 1997]. Anisotropy in this particular layer may therefore result from an array of cracks that opened during this remote period, dominantly in the plan perpendicular to the least compressive stress σ_3. Those cracks may have been further filled by melt produced by the heating that accompanied the extension and that triggered magmatic activity in this region [*Gans*, 1997]. After the cease of large tectonism in middle Miocene and the cooling of the lithosphere, this structure may have been conserved. The interpretation of the deepest anisotropic layer of the stack in our model is less straightforward. The fact that the azimuths of the axes of symmetry of the two anisotropic layers are perpendicular may be indicative of some kind of relation between the processes that generated anisotropy in these layers. A way to reconcile the apparent inconsistency is to invoke a distinct source for the anisotropy in the stack's lower layer, though controlled by the same stress setting. In particular, anisotropy in this layer located in the intermediate crust may be rather foliation-induced and the change of anisotropic source may correspond to the brittle-ductile transition. Extending the previous reasoning and assuming that the WSW-ENE oriented extension occurred in pure shear mode, foliation would develop in the plane perpendicular to the maximum compressive stress σ_1. Supposing the least compressive stress σ_3 was approximately flat, this constrains the azimuth of the foliation plane to align in the WSW-ENE direction. Given that under extension within continental crust, the magnitude of σ_1 is typically similar to that of the intermediate compressive stress σ_2, the orientation of the former and thus the dip of the foliation plane are not straightforward and may be neither vertical nor horizontal. This last point may explain the inclination of the symmetry axis of the stack's lower layer of our model. On the other hand, the dip of the symmetry axis in the upper layer of the stack indicates that the cracks' plane is not vertical. This is possibly due to the combination of pure and simple shear modes during the period of Oligo-Miocene extension. Other explanation is the possible inclination of the blocks that contain the array of cracks, posterior to the cooling of the melt that filled them.

[34] At NE81, the anisotropic zone that we modeled in the middle crust is likely to result from an oriented fabric produced by the NE-SW to ENE-WSW Oligo-Miocene extension in this area [*Nourse et al.*, 1994; *Gans*, 1997]. A similar ENE-WSW fast direction in the upper mantle was reported by *Obrebski et al.* [2006] in the northeastern GoC (including station NE81) and also by *Van Benthem et al.* [2006] in southeastern GoC. These authors propose that the fossil fabric, possibly acquired by the lithosphere during the pulse of extension mentioned above, may explain the characteristics of upper mantle anisotropy in this area. Thus the model obtained here for the crust below NE81 lends additional credence to the interpretation put forward by *Obrebski et al.* [2006] and *Van Benthem et al.* [2006]. The comparatively slower rate of recent extension in this region [*Nourse et al.*, 1994; *Gans*, 1997; *Suter and Contreras*, 2002] may account for the conservation of the Oligo-Miocene rock fabric.

6. Conclusions

[35] We obtained encouraging results at three stations located in the three structural provinces that comprise the north and central part of the Baja California Peninsula and Sonora, respectively. The transverse component of the RF exhibits unambiguous and anomalous phases that are not consistent with a significant dip of the Moho discontinuity or scattering sources. Thus, the features observed on the transverse component can be explained as due to anisotropy effects. We manage to model the main features displayed by the RFs on the radial and transversal components with good fidelity at NE71 and NE75. For station NE81 the fit

between observed and synthetic RFs is not that good, but the main tendencies are well captured. Given the difficulty that represents performing a rigorous inversion of receiver functions in an anisotropic medium, the results were obtained by forward modeling and thus are likely to be intrinsically nonunique.

[36] The three anisotropic structures that we proposed are markedly different. At NE71, an anisotropic layer is modeled in the upper crust. We propose that the anisotropy of this layer is generated by foliation in the batholith that outcrops at this site [*Gastil et al.*, 1975]. We also modeled anisotropy beneath the crust that is roughly consistent with regional E-W fast direction obtained from teleseismic shear wave splitting analysis. This anisotropy could be related to the fossil fabric of the lithosphere acquired during the subduction of Farallon, to the eastward sinking of the Farallon fragments or to the collapse of the dense lithospheric root of the former arc.

[37] At NE81, we modeled the main features of the observed RFs by stacking two anisotropic layers in the middle crust, the source of which are structurally distinct but seems to be consistent with Miocene extension. *Obrebski et al.* [2006] and *Van Benthem et al.* [2006] proposed a similar tectonic source for upper mantle anisotropy, suggesting that the whole lithosphere deformed coherently.

[38] The model proposed for NE75, located in the central part of the Baja California Peninsula, suggests the presence of metamorphosed oceanic crust about 5 km beneath the continental crust. This may constitute one of the few evidences of the presence of stalled segment of the extinct Farallon plate under the Baja California Peninsula, east of the former trench. In contrast, the anisotropic structure beneath station NE71 in the northern part of the peninsula is not indicative of the presence of the slab in the first 65 km of the lithosphere. The results of our analysis suggest therefore that the structure of the lithosphere exhibits substantial variation along the Baja California Peninsula and in particular that plate capture did not occur uniformly. This last point may carry important implications for the along axis morphology variations documented previously in the rift.

[39] More data are required to warrant further interpretations, and these first results motivate an extension of our study along the whole former trench to map areas of possible plate capture and formation of slab windows that will help to understand the structural features that make up the continental borderland and the Gulf Extensional Province.

[40] **Acknowledgments.** We acknowledge Donald Forsyth, Martha Savage, and an anonymous reviewer for their attentive revision of this manuscript. We also acknowledge John Fletcher for his comments about the interpretation of the models. The operation and data acquisition from the NARS-Baja array have been possible thanks to Arturo Pérez-Vertti, Arie van Wettum, Robert Clayton, and Jeannot Trampert. We also acknowledge the participation of Antonio Mendoza, Luis Inzunza, and Hanneke Paulssen. One of us (M.O.) was partially supported by a scholarship from the Mexican Secretaria de Relaciones Exteriores (SRE).

References

Aki, K. (1973), Scattering of P waves under the Montana Lasa, *J. Geophys. Res.*, *78*(8), 1334–1346.

Ammon, C. J. (1991), The isolation of receiver effects from teleseismic P waveforms, *Bull. Seismol. Soc. Am.*, *81*(6), 2504–2510.

Aragón-Arreola, M. J., M. T. Morandi-Soana, J. A. Martín-Barajas, L. A. Delgado-Argote, and A. González-Fernández (2005), Structure of the rift basins in the central Gulf of California: Kinematics implication for oblique rifting, *Tectonophysics*, *409*, 19–38.

Atwater, T. (1989), Plate tectonic history of the Northeast Pacific, in *The Geology of North America*, vol. N, *The Eastern Pacific and Hawaii*, edited by D. Winterer, M. Hussong, and R. W. Decker, pp. 21-72, Geol. Soc. of Am., Boulder, Colo.

Babuška, V., and M. Cara (1991), *Seismic Anisotropy in the Earth, Mod. Approaches Geophys*., vol. 10, 213 pp., Kluwer Acad., Dordrecht, Netherlands.

Bennett, S., M. Oskin, and A. Iriondo (2007), Transition from proto-gulf extension to transtension, coastal Sonora, Mexico, *Eos Trans. AGU*, *88*(23), Jt. Assem. Suppl, Abstract S31A-10.

Bohannon, R. G., and T. Parsons (1995), Tectonic implications of post-30 Ma Pacific and North American relative plate motions, *Geol. Soc. Am. Bull.*, *107*, 937–959.

Cassidy, J. F. (1992), Numerical experiments in broadband receiver function analysis, *Bull. Seismol. Soc. Am.*, *82*, 1453–1474.

Clayton, R. W., and R. A. Wiggins (1976), Source shape estimation and disconsolation of teleseismic bodywaves, *Geophys, J. R. Astron. Soc.*, *47*, 151–177.

Cochran, E. S., Y. G. Li, and J. E. Vidale (2006), Anisotropy in the shallow crust observed around the San Andreas Fault before and after the 2004 M 6.0 Parkfield earthquake, *Bull. Seismol. Soc. Am.*, *96*(4B), S364–S375, doi:10.1785/0120050804.

Crampin, S., and J. Lovell (1991), A decade of shear-wave splitting in the Earth's crust: What does it mean? What use can we make of it? and What should we do next?, *Geophys. J. Int.*, *107*, 387–407.

Dorsey, R. J., R. Castro, J. Fletcher, D. Lizarralde, and P. J. Umhoefer (2006), Report on RCL Cortez Workshop: Lithospheric rupture in the Gulf of California-Salton Trough region, *MARGIN Newsl.*, *16*, 9–13.

Farra, V., L. P. Vinnik, B. Romanowicz, G. L. Kosarev, and R. Kind (1991), Inversion of teleseismic S particle motion for azimuthal anisotropy in the upper mantle: a feasibility study, *Geophys. J. Int.*, *106*, 421–431.

Fletcher, J. M., and L. Munguía (2000), Active continental rifting in southern Baja California, México: Implications for plate-motion partitioning and the transition to seafloor spreading in the Gulf of California, *Tectonics*, *19*(6), 1107–1123.

Fletcher, J. M., M. Grove, D. L. Kimbrough, O. Lovera, and G. E. Gehrels (2007), Ridge-trench interactions and the Neogene tectonic evolution of the Magdalena Shelf and southern Gulf of California: Insights from detrital zircon U-Pb ages from the Magdalena Fan and adjacent areas, Geol, *Soc. Am. Bull.*, *119*(11), 1313–1336, doi:10.1130/B26067.1.

Gans, P. B. (1997), Large-magnitude Oligo-Miocene extension in southern Sonora: Implications for the tectonic evolution of northwest Mexico, *Tectonics*, *16*(3), 388–408.

Gastil, R. G., R. P. Phillips, and E. C. Allison (1975), Reconnaissance geology of the state of Baja California, *Mem. Geol. Soc. Am.*, *140*, 170.

Godfrey, N. J., N. I. Christensen, and D. A. Okaya (2000), Anisotropy of schists: Contribution of crustal anisotropy to active source seismic experiments and shear wave splitting observations, *J. Geophys. Res.*, *105*, 27,991–28,007.

González, M., and L. Munguía (2003), Seismic anisotropy observations in the Mexicali valley, Baja California, México, *Pure Appl. Geophys.*, *160*, 2257–2278.

Harder, S., and G. R. Keller (2000), Crustal structure determined from a new wide-angle seismic profile in southwestern New Mexico, in *Southwest Passage-A Trip Through the Phanerozoic*, edited by T. F. Lawton, N. J. McMillan, and V. T. McLemore, *Field Conf. Guideb. N. M. Geol. Soc., 51st*, 75-78.

Jung, H., and S. I. Karato (2001), Water-Induced fabric transitions in olivine, *Science*, *293*, 1460–1463.

Keith, C. M., and S. Crampin (1977a), Seismic body waves in anisotropic media: reflection and refraction at a plane interface, *Geophys. J. R. Astron. Soc.*, *49*, 181–208.

Keith, C. M., and S. Crampin (1977b), Seismic body waves in anisotropic media: propagation through a layer, *Geophys. J. R. Astron. Soc.*, *49*, 209–223.

Keith, C. M., and S. Crampin (1977c), Seismic body waves in anisotropic media: synthetic seismograms, *Geophys. J. R Astron. Soc.*, *49*, 225–243.

Langston, C. A. (1977), The effect of planar dipping structure on source and receiver responses for constant ray parameter, *Bull. Seismol. Soc. Am.*, *67*, 1029–1050.

Levin, V., and J. Park (1997), P-SH conversions in a fault-layered medium with anisotropy of arbitrary orientation, *Geophys. J. Int.*, *131*, 253–266.

Levin, V., and J. Park (1998), P-SH conversions in layered media with hexagonally symmetric anisotropy: A cookbook, *Pure Appl. Geophys.*, *151*, 669–697.

Levin, V., L. Margheriti, J. Park, and A. Amato (2002a), Anisotropic seismic structure of the lithosphere beneath the Adriatic coast of Italy constrained with mode-converted body waves, *Geophys. Res. Lett.*, *29*(22), 2058, doi:10.1029/2002GL015438.

Levin, V., J. Park, J. Lees, M. T. Brandon, V. Peyton, E. Gordeev, and A. Ozerov (2002b), Crust and upper mantle of Kamchatka from teleseismic receiver functions, *Tectonophysics*, *358*, 233–265.

Lewis, J. L., S. M. Day, H. Magistrale, R. R. Castro, L. Astiz, C. J. Rebollar, J. Eakins, F. L. Vernon, and J. N. Brune (2001), Crustal thickness of the peninsular ranges and gulf extensional province in the Californias, *J. Geophys. Res.*, *106*, 13,599–13,611.

Lonsdale, P. (1989), Geology and tectonic history of the Gulf of California, in *The Geology of North America*, vol. N, *The Eastern Pacific Ocean and Hawaii*, edited by E. L. Winterer et al., pp. 499–521, Geol. Soc. of Am., Boulder, Colo.

López-Pineda, L., C. J. Rebollar, and L. Quintanar (2007), Estimates of crustal thickness of Baja California, Sonora and Sinaloa, Mexico, using disperse surface waves, *J. Geophys. Res.*, *112*, B04308, doi:10.1029/2005JB003899.

Markee, A., and J. Gaherty (2006), Upper-mantle shear-velocity structure beneath the Gulf of California, *Eos Trans. AGU*, *87*(52), Fall Meet. Suppl., Abstract T41D-1596.

McNamara, D. E., and T. J. Owens (1993), Azimuthal shear wave velocity anisotropy in the Basin and Range Province using Moho Ps converted phases, *J. Geophys. Res.*, *98*, 12,003–12,017.

Nava, F. A., and J. N. Brune (1982), An earthquake-explosion reversed refraction line in the Peninsular Ranges of southern California and Baja California Norte, *Bull. Seismol. Soc. Am.*, *72*, 1195–1206.

Nourse, J. A., T. H. Anderson, and L. T. Silver (1994), Tertiary metamorphic core complexes in Sonora, *Tectonics*, *13*, 1161–1182.

Obrebski, M., R. Castro, R. Valenzuela, S. Van Benthem, and C. Rebollar (2006), Shear-wave splitting observations at the regions of northern Baja California and southern Basin and Range in Mexico, *Geophys. Res. Lett.*, *33*, L05302, doi:10.1029/2005GL024720.

Oskin, M., J. M. Stock, and A. Martín-Barajas (2001), Rapid localization of Pacific-North America plate motion in the Gulf of California, *Geology*, *29*(5), 459–463.

Owens, J. (1987), Crustal structure of the Adirondacks determined from broadband teleseismic waveform modeling, *J. Geophys. Res.*, *92*, 6391–6402.

Özalaybey, S., and M. K. Savage (1995), Shear-wave splitting beneath western United States in relation to plate tectonics, *J. Geophys. Res.*, *100*, 18,135–18,149.

Park, J. (1996), Surface waves in layered anisotropic structures, *Geophys. J. Int.*, *126*, 173–184.

Park, J., H. Yuan, and V. Levin (2004), Subduction-zone anisotropy under Corvallis, Oregon: A serpentinite skidmark of trench-parallel terrane migration?, *J. Geophys. Res.*, *109*, B10306, doi:10.1029/2003JB002718.

Peng, X., and E. D. Humphreys (1997), Moho dip and crustal anisotropy in northwestern Nevada from teleseismic receiver functions, *Bull. Seismol. Soc. Am.*, *87*, 745–754.

Persaud, P., X. Pérez-Campos, and R. W. Clayton (2007), Crustal thickness variations in the margins of the Gulf of California from receiver functions, *Geophys. J. Int.*, *170*(2), 687–699, doi:10.1111/j.1365-246X.2007.03412.x.

Polet, J., and J. Kanamori (2002), Anisotropy beneath California: shear wave splitting measurements using a dense broadband array, *Geophys. J. Int.*, *149*(2), 313–327, doi:10.1046/j.1365-246X.2002.01630.x.

Romo, J. M. (2002), Conductividad eléctrica de la litósfera de Baja California en la región de Vizcaí B. C. S., Ph.D., CICESE, Ensenada, Baja California.

Savage, M. K. (1998), Lower crustal anisotropy or dipping boundaries? Effects on receiver functions and a case study in New Zealand, *J. Geophys. Res.*, *103*, 15069–15,087.

Savage, M. K. (1999), Seismic anisotropy and mantle deformation: what have we learned from shear wave splitting?, *Rev. Geophys.*, *37*, 65–106.

Savage, M., J. Park, and H. Todd (2007), Velocity and anisotropy structure at the Hikurangi subduction margin, New Zealand from receiver functions, *Geophys. J. Int.*, *168*, doi:10.1111/j.1365-246X.2006.03086.x.

Sedlock, R. L. (2003), Geology of the Baja California peninsula and adjacent areas, *Spec. Pap. Geol. Soc.*, 374.

Silver, P. G., and W. W. Chan (1991), Shear wave splitting and subcontinental mantle deformation, *J. Geophys. Res.*, *96*, 16,429–16,454.

Silver, P., and M. Savage (1994), The interpretation of shear wave splitting parameters in the presence of two anisotropic layers, *Geophys. J. Int.*, *119*, 949–963.

Stock, J. M., and K. V. Hodges (1989), Pre-Pliocene extension around the gulf of California and the transfer of Baja California to the pacific plate, *Tectonics*, *8*, 99–115.

Stock, J. M., A. Martín-Barajas, F. Suárez-Vidal, and M. M. Miller (1991), Miocene to Holocene extensional tectonics and volcanic stratigraphy of the northeastern Baja California, México, in *Geological Excursions in the Southern California and México*, edited by M. J. Walawender and B. B. Hanan, pp. 44–67, Geol. Soc Am., Boulder, Colo.

Suter, M., and J. Contreras (2002), Active tectonics of northeastern Sonora, Mexico (southern Basin and Range Province) and the May 1887 M_w 7.4 earthquake, *Bull. Seism. Soc. Am.*, *92*, 581–589.

Sutherland, F. H., G. M. Kent, A. J. Harding, P. Umhoefer, D. Lizarralde, W. S. Holbrook, G. Axen, J. Fletcher, and A. González-Fernández (2006), Mid-Miocene to early Pliocene upper crustal extension in the southern Gulf of California, Eos Trans. AGU, 87 (52), *Fall Meet. Suppl.*, *87*(52), Abstract T41D-1608.

Trampert, J., H. Paulssen, A. van Wettum, J. Ritsema, R. Clayton, R. Castro, C. Rebollar, and A. Perez-Vertti (2003), New array monitors seismic activity near Gulf of California, Mexico,, *Eos Trans. AGU*, *84*(4), 29.

Umhoefer, P. F., R. J. Dorsey, and P. Renne (1994), Tectonics of the Pliocene Loreto basin, Baja California Sur, Mexico, and evolution of the Gulf of California, *Geology*, *22*, 649–652.

Van Benthem, S., R. W. Valenzuela, M. Obrebski, and R. Castro (2006), Upper mantle shear wave anisotropy under stations around the southern Gulf of California, paper presented at MARGINS Rupturing Continental Lithosphere Workshop on Lithospheric Rupture in the Gulf of California-Salton Trough Region, MARGINS-NSF Program, Ensenada, Baja California.

Yang, Y., and D. W. Forsyth (2006), 3-D tomography of the Gulf of California extensional province by Rayleigh wave inversion, , *87*(52), Fall Meet. Suppl., Abstract T41D-1595.

Zandt, G., H. Gilbert, T. J. Owens, M. Ducea, J. Saleeby, and C. H. Jones (2004), Active foundering of a continental arc root beneath the southern Sierra Nevada in California, *Nature*, *431*, 41–46.

Zhang, S., and S. I. Karato (1995), Lattice preferred orientation of olivine aggregates deformed in simple shear, *Nature*, *375*, 774–777.

Zhang, X., H. Paulssen, S. Lebedev, and T. Meier (2006), Surface wave tomography beneath the Gulf of California rift zone, *Eos Trans. AGU*, *87*(52), Fall Meet. Suppl., Abstract T41D-1594.

Zhang, X., H. Paulssen, S. Lebedev, and T. Meier (2007), Surface wave tomography of the Gulf of California, *Geophys. Res. Lett.*, *34*, L15305, doi:10.1029/2007GL030631.

Zúñiga, F. R., R. R. Castro, and T. Dominguez (1995), Stress orientation and anisotropy based on shear-wave splitting observations in the Cerro Prieto fault area, Baja California, Mexico, *Pure Appl. Geophys.*, *144*, 39–57.

R. R. Castro, CICESE, División Ciencias de la Tierra, Departamento de Sismología, km 107 Carretera Tijuana-Ensenada, Ensenada, Baja California, 22860, México.

M. Obrebski, Laboratoire de Sismologie, Institut de Physique du Globe de Paris, Boite 89, 4 place Jussieu, F-75252 Paris cedex 05, France. (obrebski@ipgp.jussieu.fr)